Systems pharmacology of the amyloid cascade : unfolding oligomer modulation in Alzheimer's disease

Maanen, E.M.T. van

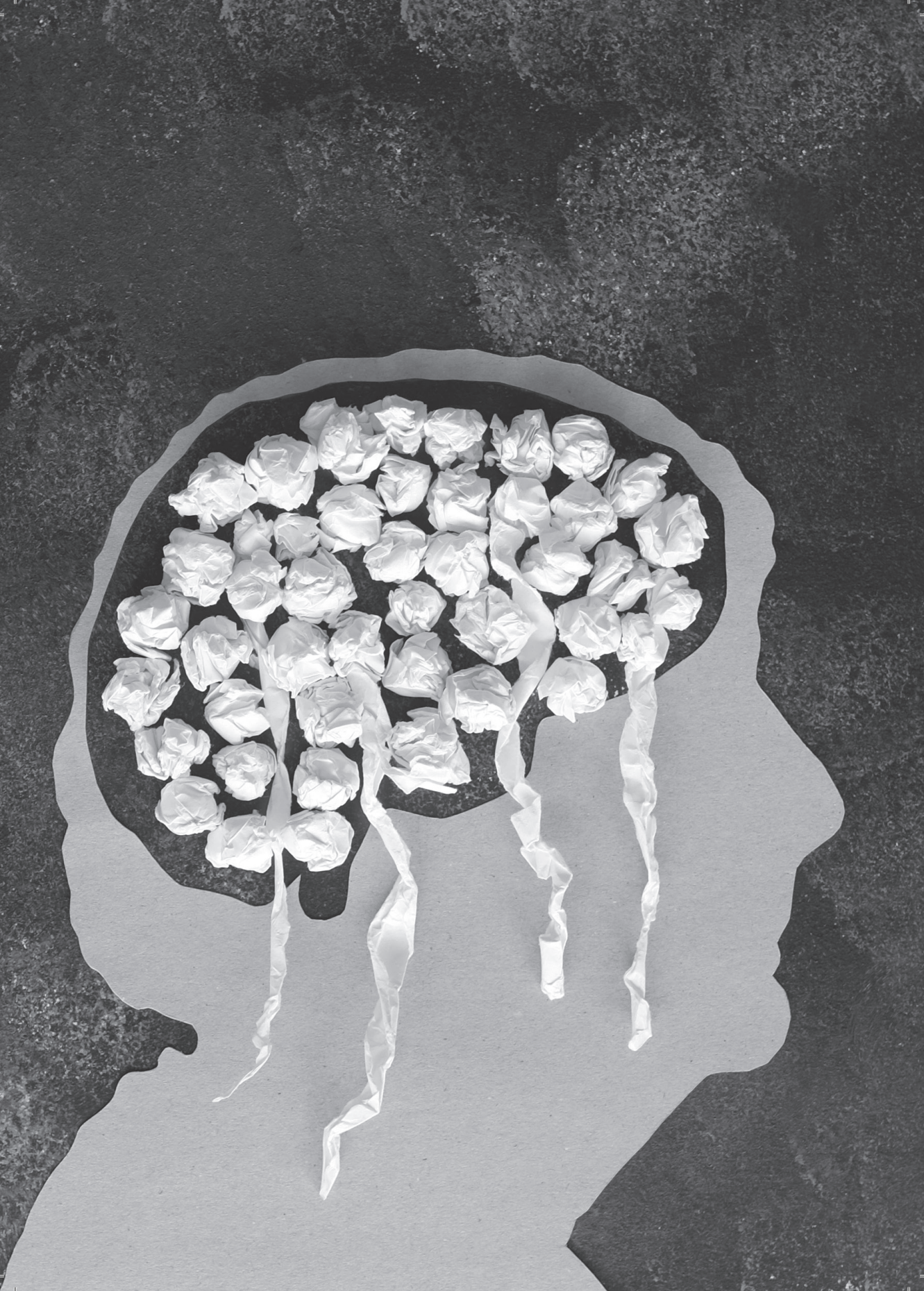

Section III

Application of a systems pharmacology model to characterize oligomer modulation following secretase inhibition

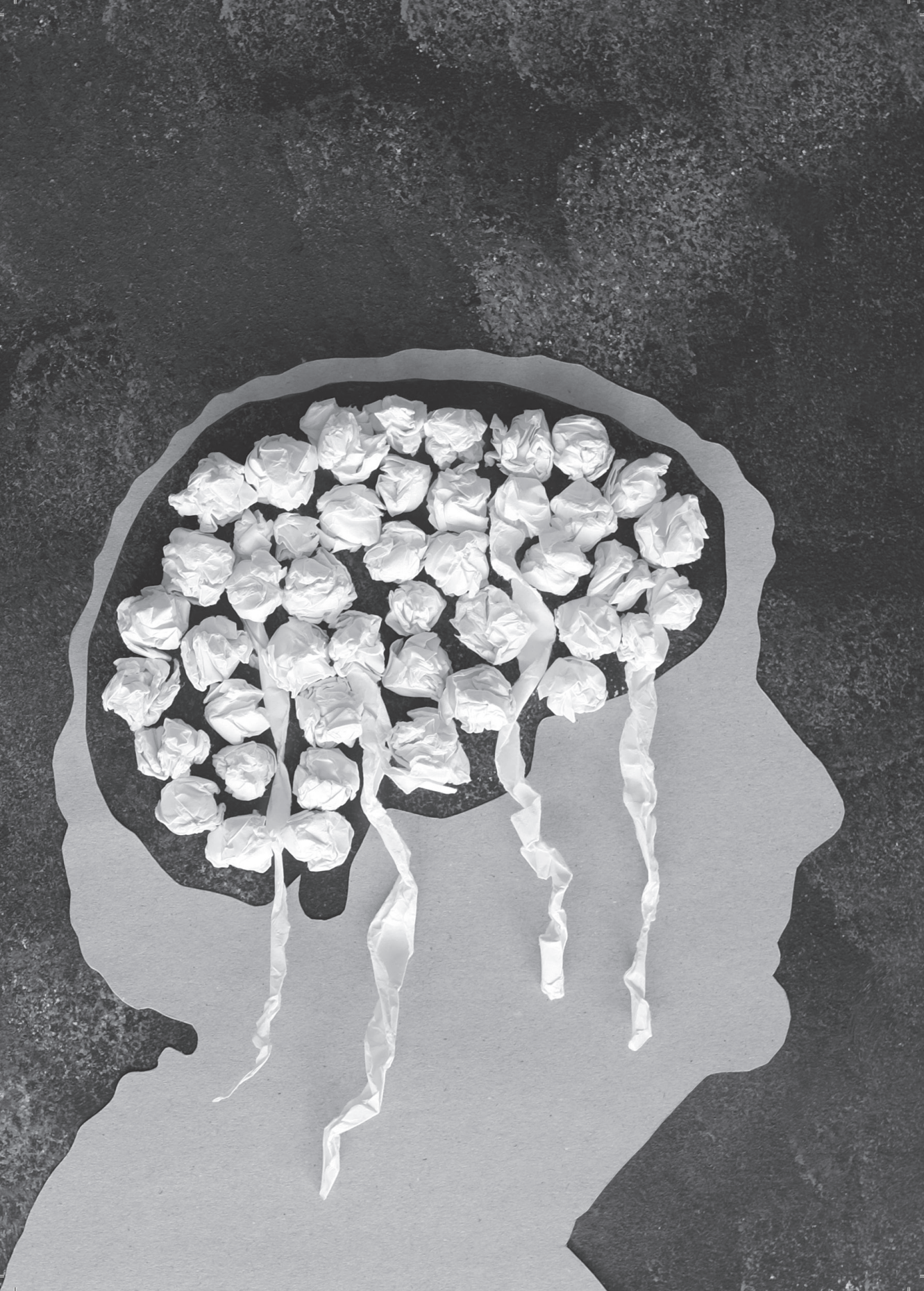

Chapter 6

Systems pharmacology analysis of the Aβ oligomer response following γ-secretase inhibition: Evidence for second-order kinetics of Aβ42 oligomerization

E.M.T. van Maanen, T.J. van Steeg, J. Kalinina, M.S. Michener,
M.J. Savage, M.E. Kennedy, J.A. Stone, M. Danhof

Abstract

Toxic soluble Aβ oligomers (Aβ_{O}) are considered to be the primary drivers of the neurodegeneration in Alzheimer's Disease (AD). Here, for the first time, the effect of BACE1 inhibition on the time course of the changes in Aβ_{O} is determined. Administration of the BACE1 inhibitor MBi-5 (30 or 125 mg/kg) resulted in a reduction of Aβ_{O} concentrations. The amyloid precursor protein (APP) metabolite (sAPPβ, sAPPα, Aβ40, Aβ42, Aβ38) and Aβ_{O} responses in CSF from cisterna-magna-ported rhesus monkeys was analysed on the basis of a recently established systems pharmacology model of the APP pathway.

The changes in Aβ_{O} were linked to the dynamics of the precursor Aβ42: There was no contribution from the precursors Aβ40 and Aβ38 to the Aβ_{O} pool. Aβ42 oligomerization was characterized to be a second-order process. Decreases in monomeric Aβ42 responses following from BACE1 inhibition were partially compensated by dissociation of Aβ_{O}. The model gave an accurate description of the 6 biomarkers. The systems pharmacology analysis provided insights into Aβ_{O} reduction after treatment with a BACE1 inhibitor, and supports the hypothesis that Aβ42 is the Aβ species prone to oligomerization. Simulations visualized that 30% reduction of the Aβ42 monomeric level reduced Aβ_{O} by more than half.

Introduction

According to the amyloid hypothesis, proteolytic processing of amyloid precursor protein (APP) to form the amyloid-β (Aβ) peptides plays a central role in the pathophysiology of Alzheimer's Disease (AD)[1,2]. Aβ levels are increased early in the disease process, while patients remain clinically asymptomatic, forming toxic soluble Aβ oligomers (Aβ_{O}) and plaques. Aβ_{O} are considered to be a primary driver of the neurodegeneration in AD brain[3].

Aβ is the final product of proteolytic cleavage of the transmembrane APP in the amyloidogenic pathway and is assumed to be a precursor of Aβ_{O}. In the APP processing and clearance pathways, APP is cleaved sequentially by β-secretase 1 (BACE1) and γ-secretase[4]. BACE1 cleavage of APP releases the N-terminal secreted fragment soluble β-amyloid precursor protein (sAPPβ) and C99, a C-terminal fragment which remains membrane bound. C99 is subsequently cleaved by γ-secretase, creating Aβ peptides of different amino acid chain lengths, of which the most common have 38, 40 or 42 amino acids (Aβ38, Aβ40, or Aβ42, respectively)[5]. A third secretase, α-secretase cleaves APP within the Aβ sequence generating non-amyloidogenic soluble sAPPα and precluding Aβ generation[6].

Aβ appears to aggregate into at least three different states: Aβ_{O}, which are soluble disordered clusters, protofibrils, which are prefibrilar insoluble high molecular weight Aβ_{O} (50-1500 kDa) comprising spherical, annular, and curvilinear assemblies, and fibrils, which are long, many-chain highly structured β-sheet-like aggregates[7,8,9]. Aβ is believed to co-exist with Aβ_{O}, protofibrils and fibrils at equilibrium[10]. The pathway by which normal monomeric forms of Aβ become fibrils is still uncertain[11].

One of the main therapeutic strategies for AD is to reduce Aβ in the central nervous system and thereby, theoretically, preventing all downstream pathological processes. Potential therapies include inhibition of the secretases responsible for its production (BACE1 or γ-secretase inhibitors). The effect of inhibiting Aβ production on Aβ_{O}s is not fully understood.

Several studies on the pharmacokinetics (PK) and the pharmacodynamics (PD) of BACE1 and γ-secretase inhibitors have been reported[12,13,14,15,16,17]. Such models focus primarily on the drug effect on Aβ40 and/or Aβ42 dynamics. A quantitative characterization of the drug effects on Aβ_{O} is still lacking.

The drug effects on the individual attributes of the APP pathway are difficult to predict, because it involves a complicated biological network. In order to develop a model that

fully characterized the drug effects on Aβ monomeric and oligomeric levels, its important to consider the interactions between APP metabolites.

Systems pharmacology provides a mathematical framework for integrating understanding of biochemical/pathological pathways with basic principles of PK and PD. Recently, a systems pharmacology model of the APP processing pathway was developed to characterize APP metabolite (sAPPβ, sAPPα, Aβ40, Aβ42) responses to BACE1 inhibition[18]. Throughout the article the name 'β-APP model' is used to refer this model. Using information from monomeric Aβ species, an Aβ42 oligomer pool was identified in the β-APP model. It is of interest to know if the Aβ_{O} response to BACE1 inhibition was correctly derived from Aβ monomeric responses. This would verify monomeric Aβ as good predictor of Aβ_{O} response to Aβ production inhibition. To this end, Aβ_{O} measurements need to be compared to model predicted Aβ_{O} levels.

In the current crossover study in cisterna-magna-ported rhesus monkeys the effects of a BACE1 inhibitor (MBi-5; 30, 125 mg/kg) on the CSF concentrations of six biomarkers (sAPPβ, Aβ40, Aβ42, Aβ38, Aβ_{O}, sAPPα) were determined. Aβ_{O} concentrations in CSF were quantified using a novel two-site ELISA assay[19]. The time course of the changes in the concentration of all biomarkers were simultaneously analysed with the β-APP model. This analysis yielded predictions of the effect of MBi-5 on the Aβ_{O} concentrations (the oligomer pool). Next, these model predictions were compared to measured Aβ_{O} concentrations. Finally, the existing model was extended to include also the effect on Aβ_{O} concentrations. Specifically, the objectives of this investigation were fourfold: (i) to compare model predicted Aβ_{O} from the recently reportedβ-APP model with observations of Aβ_{O}; (ii) to characterize Aβ_{O} dynamics following BACE1 inhibition; (iii) to confirm that Aβ_{O} dissociates to restore the equilibrium between Aβ monomers and Aβ_{O}, following secretase inhibition; (iv) to investigate the relationships of Aβ40, Aβ42 and Aβ38 monomers with the Aβ_{O} pool.

Materials and Methods

Animals

All animal studies were reviewed and approved by the MSD Institutional Animal Care and Use Committee. The NIH Guide to the care and use of Laboratory Animals and the Animal Welfare act were followed in the conduct of the animal studies (Institute of Laboratory Animal Resources, National Research Council, 1996). The CMP rhesus monkey model was reported by Gilberto et al.[20]. The rhesus monkeys are chronically

implanted with catheters in the cisterna magna, facilitating repeated sampling of CSF and plasma in conscious rhesus monkeys. These rhesus monkeys were individually housed and captive-bred in a closed colony.

In this study, six male animals, weighing between 8.6 kg and 11.8 kg (mean, 9.7 kg), age at 9 years to 13 years (mean, 11 years) at time of the study were included.

Drug administration and sampling

Information on the effect of BACE1 on sAPPα, sAPPβ, Aβ40, Aβ42, Aβ38 and Aβ_{O} was obtained following a single oral administration of MBi-5 at 30, 125 mg/kg (5 mL/kg) or vehicle (0.4% methylcellulose) in a four-way full crossover study.

Plasma and CSF drug concentrations were collected at 0 (predose) and 3, 5, 7, 9, 13, 14.5, 16, 19, 22, 25, 28, 31, 49, 55, 58, 73 and 96 h postdose, resulting in 18 plasma and CSF PK samples for each monkey per treatment group. 2 mL of blood and 1 mL of CSF were collected at each time point. The concentration of MBi-5 in the plasma and CSF samples was determined using LC-MS/MS. The concentrations of sAPPα, sAPPβ, Aβ40, Aβ42, Aβ38 and Aβ_{O} were determined from CSF samples, collected at the same time points as PK samples, by established and validated ELISA-based assays (Meso Scale Diagnostics), giving 18 measurements of each biomarker for each monkey per treatment. The two-site ELISA assay used for Aβ_{O} measurement was previously described by Savage et al. [19].

PK-PD analysis

The PK and PD data were analysed with a non-linear mixed effects modelling approach utilizing the software package NONMEM (version 7.2.0[21]). In this approach, structural (fixed) effects and both intra- and interindividual variability are taken into account. Typical values of structural model parameters (population parameters, which define the average value for a parameter in a population) (θ), the variance and covariance of the interindividual variability (ω^2) and the variance of the residual error (σ^2) are estimated.

The models were compiled using Compaq Visual Fortran (version 6.6, Compaq Computer Corporation, Houston, Texas, USA) and executed on a PC equipped with an an Intel QuadCore (Intel® Core^{TM} i7 CPU860, 2.80 GHz, 3.24 GB RAM). Data management and model assessment was done using the statistical software package S-PLUS for Windows (version 8.0 Professional, Insightful Corp., Seattle, USA).

The best models were chosen based on the analysis of their obtained minimum value of the objective function (defined as minus twice the log-likelihood), the precision of

parameter estimates, and visual inspection of goodness-of-fit plots. A more detailed description of the modelling procedure was described in van Maanen et al. [18].

To evaluate the performance of the model a visual predictive check (VPC) was performed in which the median and the 90% inter-quantile range of the data simulated with the final parameter estimates were plotted together with the observations. A validated result would have close resemblance of median observed and predicted line with 90% of the observations that fall within the 90% prediction interval.

Model description

The systems model of the APP processing pathway was developed by sequential analysis of PK and PD data following administration of MBi-5. The PK model of MBi-5 was based on simultaneous analysis of plasma and CSF PK data. The PK model of MBi-5 has been reported elsewhere by van Maanen et al. [18].

The PK model adequately described the plasma and CSF concentration time profiles of MBi-5, respectively, thus the model could serve as input for PD model analysis.

The interrelationships of the absolute amounts of APP metabolite responses to BACE1 inhibition were described recently using a comprehensive systems model of the APP processing pathway [18], the so-called β-APP model. To describe the effect of the BACE1 inhibitor on Aβ38, the model had to be extended. Also, the oligomerization of Aβ was changed to a second order process.

The biomarker response profiles of MBi-5 measured in CSF were adequately described by the β-O-APP model containing compartments for seven variables: APP, sAPPβ, sAPPα, Aβ40, Aβ38, Aβ42 and Aβ_{O} (Fig. 6.2). The production of APP was believed to be zero order, i.e. a constant production of APP. It was assumed that there is no alternative proteolytic enzyme cleaving full length APP other than α-secretase and BACE1. As both sAPPβ and C99 are products of APP cleavage by BACE1, sAPPβ and C99 were presumed to follow the same kinetics and therefore sAPPβ could be used in the model as surrogate precursor for Aβ. The production of sAPPα, sAPPβ and Aβ were assumed to be first order, i.e. dependent on the concentration of its precursor. The interaction between APP, sAPPβ, sAPPα, Aβ40, Aβ38, Aβ42 and Aβ_{O} is described by Eq. 6.1 - Eq. 6.7:

$$\frac{d}{dt}APP = Rin_{APP} - (Rin\beta \times EFF + Rin\alpha) \times APP \tag{6.1}$$

$$\frac{d}{dt}sAPP\alpha = Rin\alpha \times APP - Rout_a \times sAPP\alpha \tag{6.2}$$

$$\frac{d}{dt}sAPP\beta = Rin\beta \times EFF \times APP - (Kin_{40} + Kin_{42} + Kin_{38}) \times sAPP\beta \tag{6.3}$$

$$\frac{d}{dt}A\beta_{40} = Kin_{40} \times sAPP\beta - Kout \times A\beta_{40} \tag{6.4}$$

$$\frac{d}{dt}A\beta_{38} = Kin_{38} \times sAPP\beta - Kout * A\beta_{38} \tag{6.5}$$

$$\begin{aligned}\frac{d}{dt}A\beta_{42} = {} & Kin_{42} \times sAPP\beta - Kout_{42} \times A\beta_{42} - Kpl \times (A\beta_{42})^{ALPH} \\ & + Krev \times A\beta_O / \left(\frac{MW_{A\beta 42}}{1000} \times Factor_{oligo}\right)\end{aligned} \tag{6.6}$$

$$\frac{d}{dt}A\beta_O = Kpl \times (A\beta_{42})^{ALPH} \times \frac{MW_{A\beta 42}}{1000} \times Factor_{oligo} - Krev \times A\beta_O \tag{6.7}$$

The exchange between the Aβ_{O} pool and the Aβ42 compartment is described by Eq. 6.6 and Eq. 6.7, where *ALPH* is the power of the concentration of Aβ42, $Factor_{oligo}$ is the conversion factor on Aβ_{O} and $MW_{A\beta 42}$ is the molecular weight of Aβ42. *Krev* and *Kpl* are the dissociation rate and higher-order Aβ42 oligomerization rate constant, respectively, which are dependent on the baseline values of Aβ42 and the Aβ_{O} pool (A$\beta 42_{\mathrm{base}}$ and A$\beta_{\mathrm{O\,base}}$, resp.) according to Eq. 6.8:

$$Krev = \frac{Kpl \times (A\beta_{42base})^{ALPH} \times \frac{MW_{AB42}}{1000} \times Factor_{oligo}}{A\beta_{Obase}} \tag{6.8}$$

The rate of change of APP with respect to time in the presence of the inhibitor is described by Eq. 6.1, in which the BACE1 cleavage inhibition is incorporated by the factor *EFF*.

EFF is the degree of inhibition caused by MBi-5, expressed as shown in Eq. 6.9.

$$EFF = 1 - \frac{C_{\text{target}}^{\text{GAM}} \times Imax}{C_{\text{target}}^{\text{GAM}} + IC50^{\text{GAM}}} \tag{6.9}$$

Where C_{target} is the target site concentration of MBi-5 , *IC50* the C_{target} that results in 50% inhibition of BACE1, *Imax* is the maximum response and *GAM* is the Hill coefficient. C_{target} was derived from the PK model as:

$$C_{\text{target}} = C_{\text{plasma}} \times \frac{AUC_{\text{CSF}}}{AUC_{\text{plasma}}} \tag{6.10}$$

Where AUC_{CSF} and AUC_{plasma} are the areas under the CSF and plasma concentration time curves, respectively. C_{target} is assumed to be in steady state with C_{plasma}.

It is assumed that the system is in steady state (SS) when no treatment is given *(EFF=1)*. These steady state conditions were used to derive part of the system parameters. From SS and Eq. 6.1 it follows that the source of APP *(Rin_{APP})* is:

$$Rin_{APP} = Rout_a \times sAPP\alpha_{base} + (Kin_{40} + Kin_{42} + Kin_{38}) \times sAPP\beta_{base} \tag{6.11}$$

Where APP_{base} is the baseline level of APP, which is assumed to be equal to the sum of the baseline levels of sAPPα and sAPPβ.All alternate pathways are represented by the terms for α-secretase.

Using SS conditions and Eq. 6.2 the sAPPα formation rate ($Rin\alpha$), equivalent to the α-secretase cleavage step, can be derived:

$$Rin\alpha = Rout_a \times \frac{sAPP\alpha_{base}}{APP_{base}} \tag{6.12}$$

Where sAPPα_{base} is the baseline level of sAPPα.

The sAPPβ formation rate ($Rin\beta$), equivalent to the BACE1 cleavage step, follows from SS and Eq. 6.3:

$$Rin\beta = (Kin_{40} + Kin_{42} + Kin_{38}) \times \frac{sAPP\beta_{base}}{APP_{base}} \tag{6.13}$$

Where $sAPP\beta_{\mathrm{base}}$ is the baseline level of sAPPβ.

Using SS conditions and Eq. 6.4, 6.6 and 6.5, respectively, the formation rates of Aβ40 (*Kin40*), Aβ42 (*Kin42*) and Aβ38 (*Kin38*), equivalent to γ-secretase cleavage steps, can be calculated:

$$Kin_{40} = Kin_{42} \times \frac{A\beta 40_{base}}{A\beta 42_{base}} \tag{6.14}$$

$$Kin_{42} = Kout \times \frac{A\beta 42_{base}}{sAPP\beta_{base}} \tag{6.15}$$

$$Kin_{38} = Kin_{42} \times \frac{A\beta 38_{base}}{A\beta 42_{base}} \tag{6.16}$$

Where $A\beta 40_{\mathrm{base}}$, $A\beta 42_{\mathrm{base}}$ and $A\beta 38_{\mathrm{base}}$ are the baseline levels of Aβ40, Aβ42 and Aβ38, receptively. sAPPβ_{base} is the baseline level of sAPPβ, used here as surrogate for the baseline level of C99.

The model structure includes six transit compartments (Fig. 6.2), one for each biomarker measured in CSF (sAPPα, sAPPβ, Aβ40, Aβ42, Aβ38, Aβ_{O}), to account for transport from the target site in the brain to CSF. These transit processes are described, in general, by Eq. 6.17:

$$\frac{d}{dt} xAx_{CSF} = Ktr * (xAx - xAx_{CSF}) \tag{6.17}$$

Where *Kt* is the transit rate for the particular particular APP metabolite xAx (*KtAP* for sAPPα and sAPPβ and *KtAB* for Aβ40, Aβ42, Aβ38 and Aβ_{O}).

Results

Within-study comparison

The performance of the recently reported β-APP model [18] was assessed using a 'within-study comparison': model parameter values were optimized using the current study data and then Aβ_O was predicted and compared to the observed concentrations of Aβ_O in the present study. The rationale for this analysis is that different methodologies were used for the quantitation of the PD biomarkers in the current study compared to the previous study [18]. Consequently, biomarker baseline levels and ratios changed (see Supplemental Material). When using the β-APP model and parameter values, the difference in prediction of Aβ_O and data may be caused by methodology differences or model misspecification. It is impossible to distinguish the two from each other. In the 'within-study comparison', the difference in prediction of Aβ_O and data must be related to model misspecification and the model can be optimized accordingly.

Comparison of model predicted versus observed Aβ_O concentration profiles

The β-APP model parameters were optimized on a subset of the current data, using only the biomarker data of sAPPβ, sAPPα, Aβ40 and Aβ42. Compared to the results obtained in the previous study, the estimates of the Aβ degradation rate *(Kout)* was significantly lower and transit rate for sAPPα and sAPPβ from brain to CSF *(KtrAP)* was significantly higher (*Kout*: 0.94 h^{-1} (95% CI, 0.689-1.19) and 0.304 h^{-1} (95% CI, 0.198-0.41) in previous and current study, respectively; *KtAP*: 0.0985 (95% CI, 0.0931-0.104) and 0.127 (95% CI, 0.111-0.143) in previous and current study, respectively). The IC50 of the BACE1 inhibitor MBi-5 did not change significantly.

Using the parameter values, optimized for the current study data, the CSF Aβ_O response data in the current study was predicted. For this, similar to the compartment "Observed CSF Aβ42", the compartment "Observed CSF Aβ_O" was added to the model, which represents the transport of Aβ_O from brain-to-csf (Figure 6.2). The prediction of the onset of the Aβ_O response to BACE1 inhibition was slow relative to the observations (Figure 6.1). Likewise, the maximum response was also underpredicted.

A conversion factor was included to account for different units of Aβ monomers and Aβ_O

It is to be noted that the concentrations of Aβ monomers were expressed in pM and Aβ_O concentrations were expressed in pg/mL. Therefore, a conversion factor needed

to be included in the model, which has a relationship with the molecular weight of the oligomers and other processes involved (e.g. differences in distribution volume). The conversion factor is implemented in the differential equations describing Aβ42 (Eq. 6.6) and Aβ_{O} (Eq. 6.7). Based on visual inspection, this factor was initially set to 0.05 for the prediction discussed above and later optimized to be 0.0178.

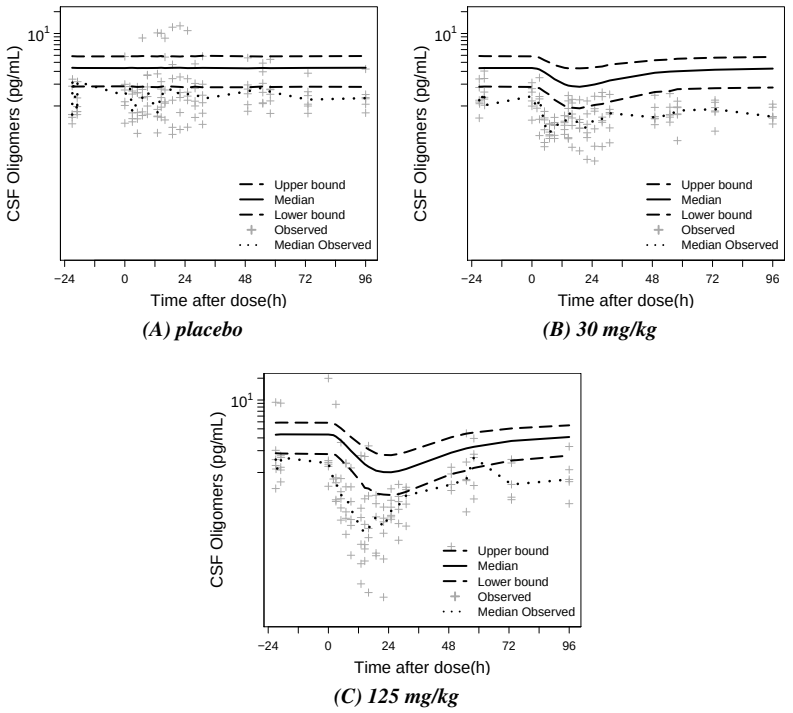

Figure 6.1: Prediction of Aβ_{O} response* vs. *time profile of placebo (A), 30 mg/kg (B) and 125 mg/kg (C) MBi-5 in the rhesus monkeys with 90% confidence interval.
Predictions were performed with the model structure presented in van Maanen et al. [18], with parameter values optimized on the current study data (*within-study comparison*). Observation sample size: n=108 for each APP metabolite from 6 monkeys collected over 4 days.
Plus-symbols represent observed measurements. Dotted line corresponds to the median observed profile. Solid lines show the median predicted profiles. The long-dashed lines correspond to the 90% prediction intervals obtained from 1000 individual simulated profiles.

The systems model was extended to describe Aβ38 response

The APP systems model was optimized, based on simultaneous analysis of sAPPβ, sAPPα, Aβ40, Aβ42, Aβ38 and $A\beta_O$ response data for BACE1 inhibition. Modifications were made to the β-APP model structure by adding extra compartments to describe Aβ38 dynamics and brain-to-csf transport, as shown in the schematic of the extended, so-called β-O-APP model, in Figure 6.2.

The differential equation representing Aβ38 dynamics in the β-O-APP model is Eq. 6.5. The same Aβ degradation rate *(Kout)* was identified for each Aβ isoform (Aβ40,

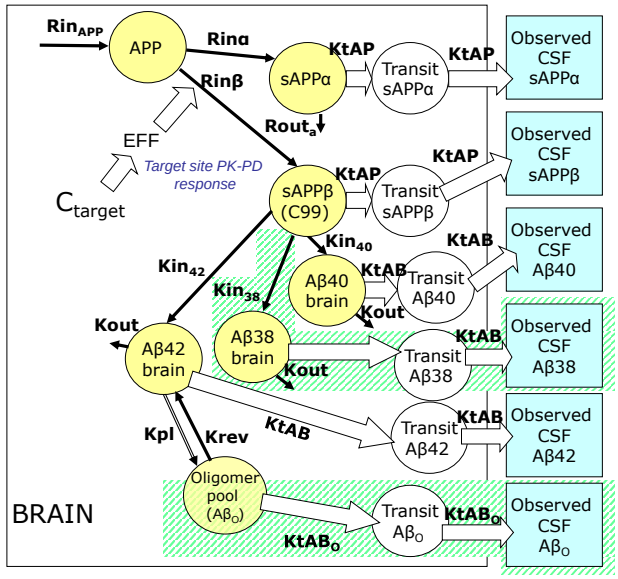

Figure 6.2: Schematic of β-O-APP model.
The model comprised thirteen compartments: Seven biomarker compartments in brain *(yellow circles)* and six transit compartments from brain to CSF *(white circles)*. Six biomarkers were measured in CSF (sAPPα, sAPPβ, Aβ40 ,Aβ42, Aβ38 and $A\beta_O$), indicated by the blue boxes. The drug effect *(EFF)* inhibited *Rinβ*. As driver of biomarker response C_{target} was used, which was derived from the PK model [18]. sAPPβ was used in the model structure as a surrogate substrate for C99 in the γ-secretase cleavage step [18]. Model extensions compared to the β-APP model presented in van Maanen et al. [18] are indicated with the green shaded area.
APP: Aβ-precursor protein; *Aβ*: amyloid-β-peptide; C_{target}: drug concentration target site; Kin_{38}: Aβ38 formation rate; Kin_{40}: Aβ40 formation rate; Kin_{42}: Aβ42 formation rate; *Kout*: Aβ38, Aβ40 and Aβ42 degradation rate; *Krev*: Oligomer dissociation rate; *KtAP*: transit rate sAPPα and sAPPβ from brain to CSF; *Kpl*: Oligomerization rate; *KtAB*: transit rate Aβ from brain to CSF; $KtAB_O$: transit rate $A\beta_O$ from brain to CSF; *RinAPP*: source of APP; *Rinα*: sAPPα formation rate; *Rinβ*: sAPPβ formation rate; *Routa*: sAPPα degradation rate.

Aβ42, Aβ38). Further, the transit rate for brain-to-CSF transport *(KtAB)* did not differ for Aβ38 compared to Aβ40 and Aβ42. Different formation rates were implemented for each one of the Aβ species. The formation rates of Aβ40, Aβ42 and Aβ38 were calculated according to Eqs. 6.14-6.16. The highest formation rate was found for Kin_{40} (1.29 h^{-1}), followed by Kin_{38} (0.380 h^{-1}) and than Kin_{42} (0.0993 h^{-1}).

Aβ42 only contributor to Aβ_O pool

After extension of the model for Aβ38, the contribution of Aβ40, Aβ38 and Aβ42 to the oligomer pool was investigated. These Aβ species were evaluated both as single contributors as combined sources of Aβ for the oligomer pool, by including oligomerization rates for each Aβ. Aβ42 was identified as the only contributor to the oligomer pool.

Aβ oligomerization is a second-order process

The dependence of the Aβ_O concentration on the Aβ42 concentration was investigated. The oligomerization was identified to be a higher order process, with an order of 1.81 (95% CI, 1.33-2.29), indicating that its rate is proportional to the $\sim$2nd power of the concentration of monomeric species and that the oligomerization can only occur when two Aβ42 peptides interact. The difference in absolute oligomer response following a 1^{st}, 1.81 and $2nd$ order oligomerization process is visualized in Figure 6.3. This plot illustrates that the order of the oligomerization process affects not only the onset of the oligomer response, but also the maximum effect.

The second-order Aβ oligomerization means that a relatively larger change from baseline for Aβ_O compared to monomeric Aβ species is obtained following BACE1 inhibition, as is depicted in Figure 6.5B.

To better understand the relationship between Aβ42 and Aβ_O response, the change of baseline for Aβ42 was plotted against the change of baseline for Aβ_O (Figure 6.4). This plot exhibits a hysteresis loop between Aβ42 and Aβ_O effects, when followed over time.

Thus, the same Aβ42 concentration corresponds to two different magnitudes of Aβ_O effects depending on the temporal sequence in which the effect is measured (e.g. 30% reduction in Aβ42 and 11% or 57% reduction in Aβ_O following 125 mg/kg MBi-5). The reason is because the maximum Aβ42 response was achieved before the maximum of Aβ_O response (Figure 6.5A).

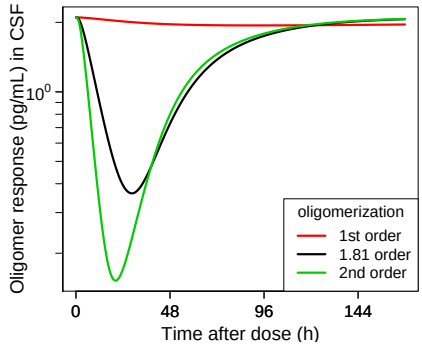

Figure 6.3: Illustration of the difference in absolute oligomer response following a 1^{st}, 1.81 and 2^{nd} order oligomerization process. The oligomer response was simulated after a single dose of 125 mg MBi-5, using the typical parameter estimates.
1^{st} order: red solid line; *1.81 order:* black solid line; *2^{nd} order:* green solid line.

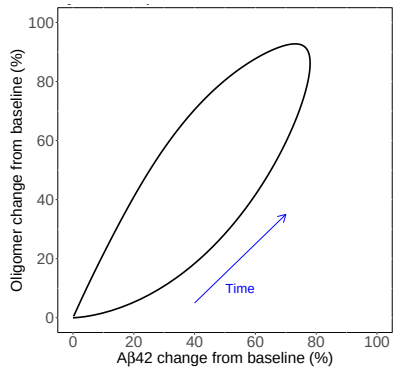

Figure 6.4: Illustration of the relationship between response of Aβ42 and Aβ_{O}. The Aβ_{O} and Aβ42 response was simulated after a single dose of 125 mg MBi-5, using the typical parameter estimates.

The β-O-APP model described APP metabolite and Aβ_{O} responses to BACE1 inhibition

Figures 6.6-6.8 show the model description of each APP metabolite and Aβ_{O} for each dose group. In general, an adequate description of the biomarker responses was obtained across dose groups. A slight underprediction was observed for sAPPβ response at dose 125 mg/kg (Figure 6.8B) and overprediction of the Aβ_{O} baseline (Figure 6.6F).

The β-O-APP model was used to simulate the biomarker interrelationships in CSF

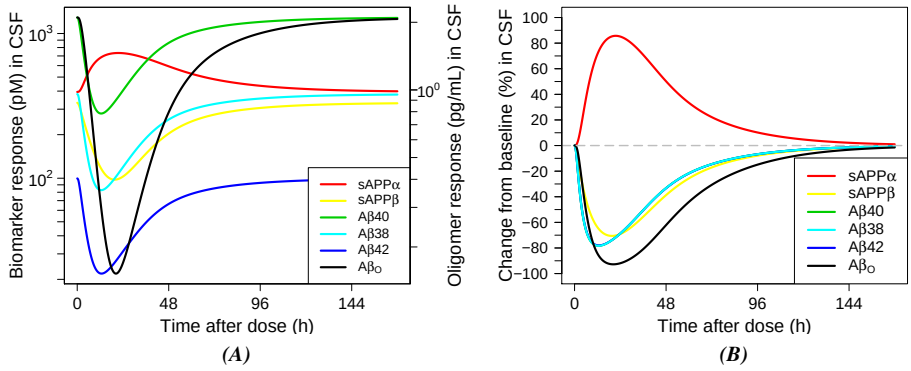

Figure 6.5: Simulation absolute biomarker responses (A) and biomarker change from baseline (%) (B). The biomarker responses were simulated after a single dose of 125 mg MBi-5, using the typical parameter estimates.
sAPPα red solid line; *sAPP*β yellow solid line; *A*β*40* green solid line; *A*β*38* light blue solid line; *A*β*42* dark blue solid line; Aβ_O black solid line.

after BACE1 inhibition (Figure 6.5A), illustrating that the biomarker maximum responses in CSF appear at different time sequence. Also, the response profiles of Aβ40, Aβ42 and Aβ38 were similar, albeit at different concentration levels. When visualizing the change from baseline for these Aβ species, the profiles were overlapping (Figure 6.5B).

Model parameters

The population parameters and intra- and interanimal variability, optimized for the current study population, are presented in Table 6.1. The random-effects model structure was optimized by comparing the results of models with interanimal variability on different parameters. The final model included interanimal variability for the baselines of sAPPβ, sAPPα and Aβ, modelled as lognormally distributed parameters. The same interanimal variability was included for the baselines of Aβ38, Aβ40 and Aβ42, as these are products of the same cleavage step. For each APP metabolite (sAPPβ, sAPPα, Aβ40, Aβ42, Aβ38, Aβ_O) separately, a proportional error was used to describe the random residual variability.

The parameter estimate of the IC50 was not significantly different from recently reported: in the recent analysis an IC50 of 0.0269 μM (95% CI, 0.0154–0.0384) was found[18]; in the current analysis an IC50 of 0.0322 μM (95% CI, 0.0214-0.043) was identified.

Table 6.1: Population parameter estimates including coefficient of variation (CV%)

PARAMETER	DESCRIPTION	VALUE	UNIT	CV%
Structural parameters				
sAPPβ_{base}	baseline sAPPβ	332	pM	24.9
Aβ38$_{\mathrm{base}}$	baseline Aβ38	381	pM	13.2
Aβ40$_{\mathrm{base}}$	baseline Aβ40	1290	pM	7.18
Aβ42$_{\mathrm{base}}$	baseline Aβ42	99.6	pM	10.3
sAPPα_{base}	baseline sAPPα	395	pM	17.5
Kout	degradation rate Aβ40, Aβ42, Aβ38	0.321	h^{-1}	14.5
Rout$_{\mathrm{a}}$	degradation rate sAPPα	1.18	h^{-1}	13.6
KtAP	transit rate sAPPα and sAPPβ	0.138	h^{-1}	5.68
KtAB[a]	transit rate Aβ	10	h^{-1}	
Imax[a]	maximal inhibition (Imax)	1		
IC$_{50}$	median inhibition concentration	0.0322	μM	17.1
GAM	Hill coefficient	0.749		10.3
Kpl	second-order oligomerization rate constant	6.59e-4	$pM^{-1}\ h^{-1}$	10.3
A$\beta_{\mathrm{O\,base}}$	baseline Aβ_{O}	2.1	pg/mL	13.8
ALPH[a]	Power of the concentration of Aβ42	2		
Factor$_{oligo}$	Conversion factor on Aβ_{O}	0.0178		45.8
Interanimal variability				
$\omega^2{}_{\mathrm{BSAPb}}$ [b]	Interanimal variability sAPPβ baseline	0.26		30.4
$\omega^2{}_{\mathrm{BSAPa}}$ [b]	Interanimal variability sAPPα baseline	0.145		30.3
$\omega^2{}_{\mathrm{AB}}$ [b]	Interanimal variability Aβ	0.103		39.8
Residual error				
$\sigma^2{}_{\mathrm{A}\beta40}$ [c]	Residual variability Aβ40	0.078		12.1
$\sigma^2{}_{\mathrm{A}\beta42}$ [c]	Residual variability Aβ42	0.0576		19.8
$\sigma^2{}_{\mathrm{sAPP}\beta}$ [c]	Residual variability sAPPβ	0.0971		26
$\sigma^2{}_{\mathrm{sAPP}\alpha}$ [c]	Residual variability sAPPα	0.0486		23.3
$\sigma^2{}_{\mathrm{oligo}}$ [c]	Residual variability Aβ_{O}	1.14		20.7
$\sigma^2{}_{\mathrm{A}\beta38}$ [c]	Residual variability Aβ38	0.0711		19.5

[a] Fixed.

[b] Interanimal variability is assumed to follow a normal distribution with mean zero and variance ω^2.

[c] Residual variability is assumed to follow a normal distribution with mean zero and variance σ^2.

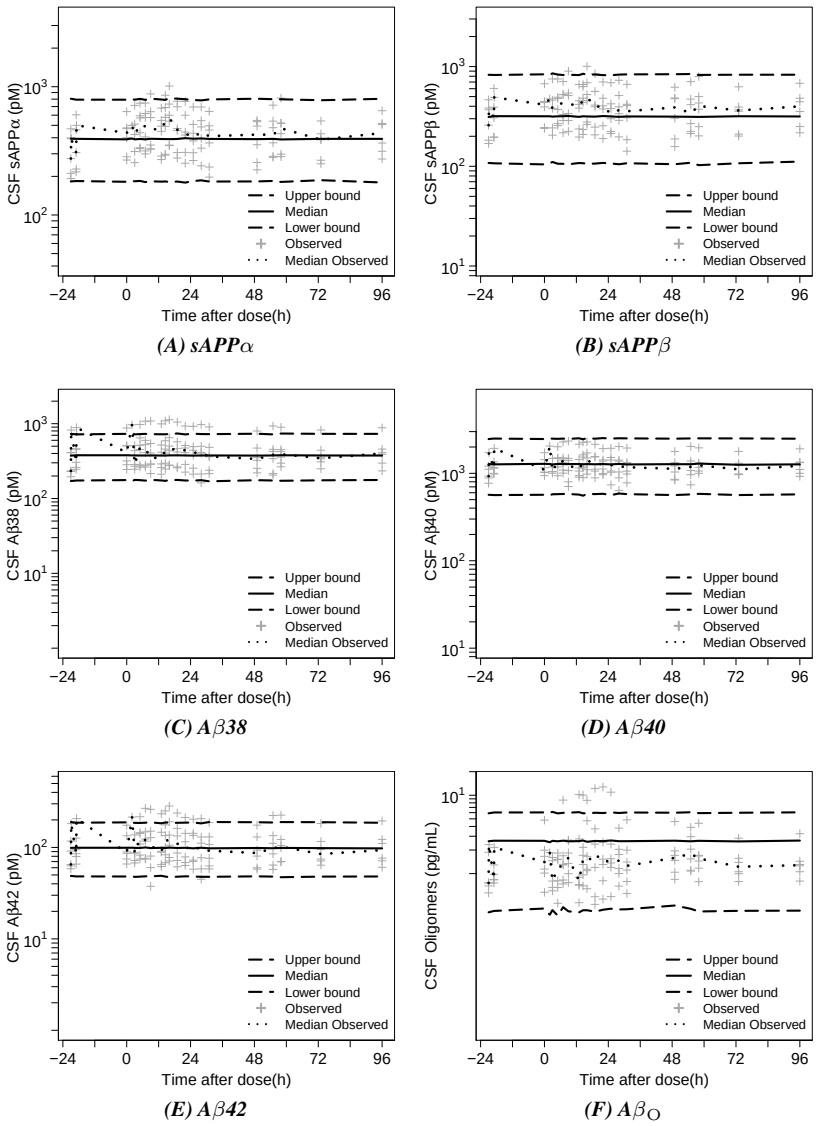

Figure 6.6: Placebo. Visual predictive check of biomarker response* vs. *time profile of placebo in the rhesus with 90% confidence interval. Predictions were performed with extended model ((A), (B), (C), (D), (E), (F)). Observation sample size: n=108 for each APP metabolite from 6 monkeys collected over 4 days.

Plus-symbols represent observed measurements. Dotted blue line corresponds to the median observed profile. Solid lines show the median simulated profiles. The long-dashed lines correspond to the 90% prediction intervals obtained from 1000 individual simulated profiles.

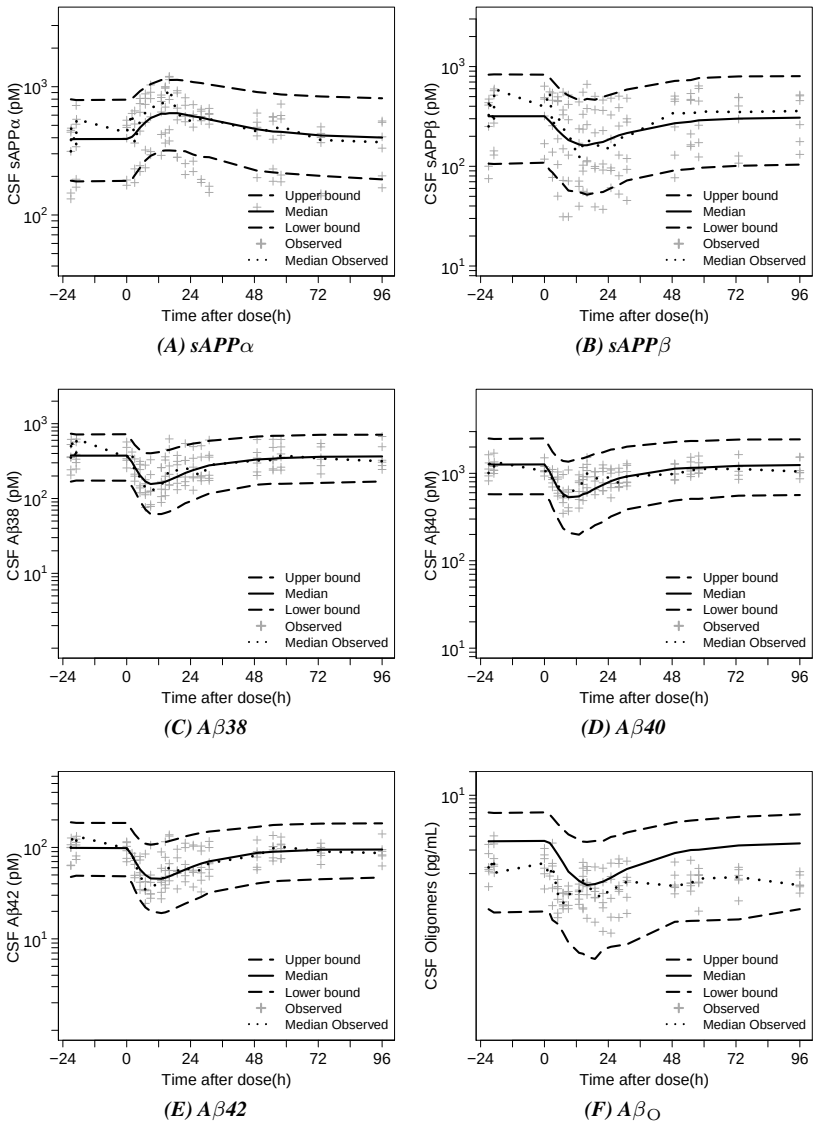

Figure 6.7: Dose 30 mg/kg. Visual predictive check of biomarker response* vs. *time profile of MBi-5 in the rhesus with 90% confidence interval. Predictions were performed with model with extended model ((A), (B),(C), (D), (E),(F)). Observation sample size: n=108 for each APP metabolite from 6 monkeys collected over 4 days.

Plus-symbols represent observed measurements. Dotted blue line corresponds to the median observed profile. Solid lines show the median simulated profiles. The long-dashed lines correspond to the 90% prediction intervals obtained from 1000 individual simulated profiles.

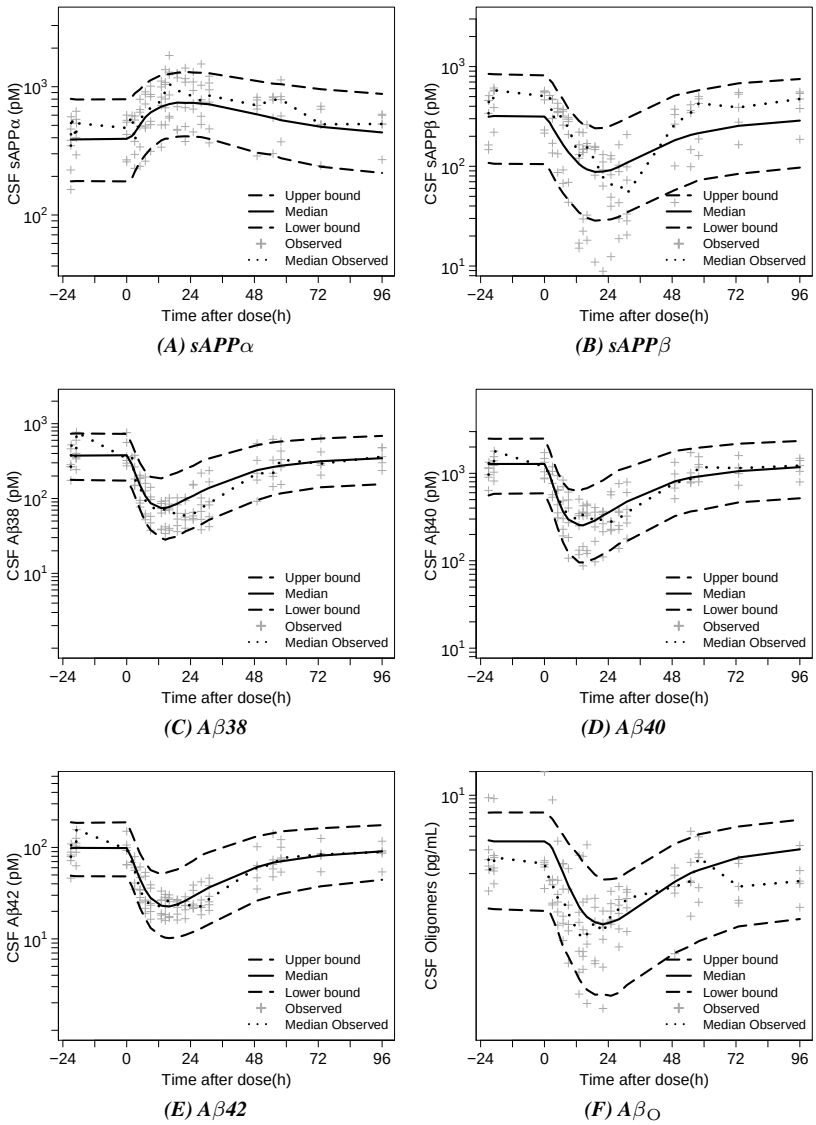

Figure 6.8: Dose 125 mg/kg. Visual predictive check of biomarker response* vs. *time profile of MBi-5 in the rhesus with 90% confidence interval. Predictions were performed with extended model ((A), (B),(C), (D), (E),(F)). Observation sample size: n=108 for each APP metabolite from 6 monkeys collected over 4 days.

Plus-symbols represent observed measurements. Dotted blue line corresponds to the median observed profile. Solid lines show the median simulated profiles. The long-dashed lines correspond to the 90% prediction intervals obtained from 1000 individual simulated profiles.

Discussion

Soluble Aβ_O are believed to be responsible for the neurodegeneration or toxicity to brain tissue observed in AD. To optimize therapeutic intervention targeting Aβ production with the aim to reduce Aβ_O burden, it is important to understand and quantify the PD effects on Aβ_O. In that respect, it is imperative to consider the behaviour of the APP system as a whole.

The recently reported APP systems model[18], the β-APP model, was extended to include Aβ38 dynamics and describe Aβ_O response data from a novel assay. The so-called β-O-APP model successfully captured sAPPβ and sAPPα concentration behaviour, Aβ monomeric (Aβ38, Aβ40, Aβ42) and oligomeric concentrations and the interactions between these species.

Aβ oligomerization was a second order process, indicating that the concentration of Aβ directly affects the rate of the reaction. Specifically, doubling the concentration of Aβ would quadruple the rate of the oligomerization. The half-life of the oligomerization process is dependent on the initial Aβ concentration. The second-order kinetics of Aβ oligomerization means that a relatively higher change from baseline for Aβ_O compared to monomeric Aβ species is obtained following BACE1 inhibition. e.g. 30% reduction in Aβ42 yields a 50% reduction in Aβ_O following 125 mg/kg MBi-5. By reducing Aβ_O levels, neuropathological alterations underlying AD may be slowed down or stopped. As such, Aβ production inhibition is a potential disease modifying therapy.

The β-O-APP model also contains expressions to account for the fact that decreases in monomeric Aβ42 response resulting from BACE1 inhibition is partially compensated by reverse dissociation of Aβ_Os. Aβ_Os appear to dissociate in order to restore the balance between Aβ monomers and Aβ_O. This supports the belief that Aβ co-exist with Aβ_O in equilibrium and that Aβ_O formation is reversible to a certain extent[10]. As amyloid plaques and fibrils might exist in equilibrium with Aβ oligomeric forms, reducing Aβ_O levels through Aβ production inhibition may bring down higher ordered forms as well. Takamura et al.[22] reported that antibodies raised against Aβ_O reduced plaques in conjunction with Aβ_O.

Our analysis indicated that of the measured Aβ species (Aβ38,Aβ40,Aβ42) Aβ42 was the only major contributor to the oligomer pool. This is in line with the findings that Aβ42 is the dominant Aβ species in plaques and fibrils[23,24,25]. Further, Garai and Frieden[26] reported greater *in vitro* oligomerization propensity of Aβ42 compared to Aβ40, using a fluorescent assay with tetramethylrhodamine-labelled Aβ. Aβ42 is very self-aggregating,

while Aβ40 may actually be anti-amyloidogenic[2,27]. The additional two amino acids on the C-terminus of Aβ42 makes the peptide more hydrophobic and significantly more rigid than Aβ40 and susceptible to aggregation. The increased rigidity promotes entropy-driven aggregation. The high hydrophobicity of Aβ42 pushes for aggregation to reduce exposure of the hydrophobic tail[28].

Recently, Aβ_{O} were predicted to decrease in response to BACE1 inhibition, which was at that time derived indirectly on the basis of an analysis monomeric Aβ response data. In the current analysis, the decrease in Aβ_{O} concentrations following BACE1 inhibition was confirmed. The within-study comparison that was used to compare model predicted versus observed Aβ_{O} indicated that the onset of the Aβ_{O} response was predicted to be slower and the predicted maximum response was lower than observed.

The addition of the parameter Factor_{olig} made it possible to account for differences in units of the quantification assays of monomeric Aβ and Aβ_{O}. This parameter has a relationship with the size of the oligomers and other process involved. A lower apparent volume of distribution of Aβ_{O} compared to Aβ monomers would be expected, if the measured Aβ_{O}s are high-molecular weight species. This would then be reflected in Factor_{orig}. The measured Aβ_{O}s were a mixture of Aβ_{O} with different number if Aβ monomers incorporated, of which the distribution was unknown. If, for simplicity, it is assumed that Factor_{orig} only has a relationship with Aβ_{O} size, it is defined as one divided by the number of subunits of Aβ42 in Aβ_{O}. This would indicate that, on average, the measured Aβ_{O}s contain 56 subunits of Aβ. This is close to the reported size of larger amyloid oligomers of 30-50 protein molecules[29].

It was not possible to use the parameter estimates from the β-APP model in the current analysis, as different biomarker assays were used to determine APP metabolite concentrations. In principle, identified system parameters are attributed to the biological system and may not change from one analysis to another[30]. However, in practice, due to experimental variation system parameters may shift. Then, it is important to understand what is measured and to realize what experimental design aspects might be different as well as those that are kept the same. With respect to the development of a system model, standardization of biomarker assays for data collection will be beneficial.

The β-APP model was extended to describe Aβ38, in addition to Aβ40 and Aβ42 dynamics. Different formation rates were found for these Aβ species. Ranking the formation rates from high to low these rank: Aβ40, Aβ38, Aβ42. This is consistent with the composition of Aβ species reported for human CSF, in which Aβ40 is the dominant isoform, and the concentration of Aβ42 was much lower than Aβ40 and Aβ38

concentrations[31].

Unwanted protein aggregation, such as that of Aβ in AD, is generally believed to involve aggregation in a non-native state. In the case of amyloidogenic proteins, the starting reactant is the monomeric form of the protein and the product of the protein aggregation is aggregated protein fibrils. The intermediate species that are formed along the way are still uncertain. Various approaches to determine protein aggregation kinetics and understand the underlying mechanism have been reported in literature and were reviewed by Morris et al.[11]. These were based on *in situ* and *ex situ* aggregation kinetics studies. Lomakin et al.[32] investigated the fibrillation of Aβ40, by following its aggregation using quasi-elastic light scattering *in vitro*. They proposed a critical protein concentration above which stepwise protein aggregation occurs: (i) monomers, (ii) micelles, (iii) nuclei, (iv) fibrils. The fiber elongation rate was proposed to be proportional to the Aβ40 monomer concentration, i.e. a first order process. This cannot be directly compared to the higher order Aβ42 oligomerization identified in the current analysis. As Aβ42 is more prone to aggregation than Aβ40 *(vide supra)*, the results reported by Lomakin et al.[32] might have been different for Aβ42 under the same experimental conditions. Moreover, *in vitro* conditions for aggregation are less complex than *in vivo*, where processes as production, elimination, deposition and fibrillization of Aβ monomers are in dynamic equilibrium.

Conclusions & Perspectives

The findings reported herein indicate that the use of systems pharmacology modelling can be a very useful tool when investigating drug effects on attributes of a complicated biological network. The β-O-APP model was able to integrate information from an Aβ_{O} assay with the PK and APP metabolites concentration measurements in response to BACE1 inhibition. This yielded important information about the relationship between monomeric Aβ species and Aβ_{O}s: (1) Oligomerization was a higher order process. This means that a relatively larger change from baseline for Aβ_{O} compared to monomeric Aβ species is obtained following BACE1 inhibition; (2) Aβ_{O}s decreased in response to BACE1 inhibition; (3) Of the measured Aβ species Aβ42 was the only major contributor to the oligomer pool.

The β-O-APP model brings us closer to optimizing the therapeutic intervention to reduce Aβ_{O} burden. In a follow-up analysis, the potential reduction of the putatively neurotoxic Aβ_{O} pool following γ-secretase inhibition will be investigated. Potential differences in effects on Aβ_{O} levels after treatment with a BACE1 *versus* a γ-secretase inhibitor will be evaluated. To this end, data following treatment with the γ-secretase inhibitor

MK-0752 from the current study will be added to further inform the model (**Chapter 7**).

References

1. Di Carlo, M., Giacomazza, D., & San Biagio, P.L. Alzheimer's disease: biological aspects, therapeutic perspectives and diagnostic tools. J physics Condens matter an Inst Phys J. 2012;24(24):244102.
2. Selkoe, D.J. & Hardy, J. The amyloid hypothesis of Alzheimer's disease at 25 years. EMBO Mol Med. 2016;8(6):595–608.
3. Klein, W.L. Synaptotoxic amyloid-β oligomers: a molecular basis for the cause, diagnosis, and treatment of Alzheimer's disease? J Alzheimer's Dis. 2013;33:S49–S65.
4. Esler, W.P. & Wolfe, M.S. A portrait of Alzheimer secretases - New features and familiar faces. Science. 2001;293(5534): 1449–54.
5. Wiltfang, J., *et al.* Higly conserved and disease-specific patterns of carboxyterminally truncated Aβ peptides 1-37/38/39 in addition to 1-40/42 in Alzheimer's disease and in patients with chronic neuroinflammation. J Neurochem. 2002;81(3):481–496.
6. Lichtenthaler, S.F. Alpha-secretase in Alzheimer's disease: Molecular identity, regulation and therapeutic potential. J Neurochem. 2011;116(1):10–21.
7. Grüning, C.S.R., *et al.* The off-rate of monomers dissociating from amyloid-β protofibrils. J Biol Chem. 2013;288(52): 37104–11.
8. Schmit, J.D., Ghosh, K., & Dill, K. What Drives Amyloid Molecules To Assemble into Oligomers and Fibrils? Biophys J. 2011;100(2):450–458.
9. Cerasoli, E., Ryadnov, M.G., & Austen, B.M. The elusive nature and diagnostics of misfolded Aβ oligomers. Front Chem. 2015;3:17.
10. Benilova, I., Karran, E., & De Strooper, B. The toxic Aβ oligomer and Alzheimer's disease: an emperor in need of clothes. Nat Neurosci. 2012;15(3):349–357.
11. Morris, A.M., Watzky, M.A., & Finke, R.G. Protein aggregation kinetics, mechanism, and curve-fitting: a review of the literature. Biochim Biophys Acta. 2009;1794(3):375–97.
12. Lu, Y., *et al.* Cerebrospinal fluid amyloid-β (Aβ) as an effect biomarker for brain Aβ lowering verified by quantitative preclinical analyses. J Pharmacol Exp Ther. 2012;342 (2):366–75.
13. Lu, Y., *et al.* Cerebrospinal fluid β-amyloid turnover in the mouse, dog, monkey and human evaluated by systematic quantitative analyses. Neurodegener Dis. 2013;12(1): 36–50.
14. Parkinson, J., *et al.* Modeling of age-dependent amyloid accumulation and γ-secretase inhibition of soluble and insoluble Aβ in a transgenic mouse model of amyloid deposition. Pharmacol Res Perspect. 2013;1 (2):e00012.
15. Janson, J., *et al.* Population PKPD modeling of BACE1 inhibitor-induced reduction in Aβ levels in vivo and correlation to in vitro potency in primary cortical neurons from

mouse and guinea pig. Pharm Res. 2014;31 (3):670–83.

16. Das, R., *et al.* Modeling effect of a γ-secretase inhibitor on amyloid-β dynamics reveals significant role of an amyloid clearance mechanism. Bull Math Biol. 2011;73 (1):230–47.

17. Niva, C., Parkinson, J., Olsson, F., van Schaick, E., Lundkvist, J., & Visser, S.a.G. Has inhibition of Aβ production adequately been tested as therapeutic approach in mild AD? A model-based meta-analysis of γ-secretase inhibitor data. Eur J Clin Pharmacol. 2013;69(6):1247–60.

18. van Maanen, E.M.T., *et al.* Systems pharmacology analysis of the amyloid cascade after β-secretase inhibition enables the identification of an Aβ42 oligomer pool. J Pharmacol Exp Ther. 2016;357(1):205–16.

19. Savage, M.J., *et al.* A sensitive Aβ oligomer assay discriminates Alzheimer's and aged control cerebrospinal fluid. J Neurosci. 2014;34(8):2884–97.

20. Gilberto, D.B., *et al.* An alternative method of chronic cerebrospinal fluid collection via the cisterna magna in conscious rhesus monkeys. Contemp Top Lab Anim Sci. 2003;42 (4):53–59.

21. Bauer, R.J. 2011 NONMEM users guide. Introduction to NONMEM 7.2.0 Technical report;ICON Development Solutions, Ellicott City, MD.

22. Takamura, A., *et al.* Sortilin is required for toxic action of Aβ oligomers (AβOs): Extracellular AβOs trigger apoptosis, and intraneuronal AβOs impair degradation pathways. Life Sci. 2012;91(23-24):1177–1186.

23. Iwatsubo, T., Odaka, A., Suzuki, N., Mizusawa, H., Nukina, N., & Ihara, Y. Visualization of Aβ42(43) and Aβ40 in senile plaques with end-specific Aβ monoclonals: evidence that an initially deposited species is Aβ42(43). Neuron. 1994;13(1):45–53.

24. Gu, L., Tran, J., Jiang, L., & Guo, Z. A new structural model of Alzheimer's Aβ42 fibrils based on electron paramagnetic resonance data and Rosetta modeling. J Struct Biol. 2016;194(1):61–67.

25. Economou, N.J., *et al.* Amyloid β-Protein Assembly and Alzheimer's Disease: Dodecamers of Aβ42, but Not of Aβ40, Seed Fibril Formation. J Am Chem Soc. 2016;138 (6):1772–1775.

26. Garai, K. & Frieden, C. Quantitative analysis of the time course of Aβ oligomerization and subsequent growth steps using tetramethylrhodamine-labeled Aβ. Proc Natl Acad Sci U S A. 2013;110(9):3321–6.

27. Kim, J., *et al.* Aβ40 Inhibits Amyloid Deposition In Vivo. J Neurosci. 2007;27(3): 627–633.

28. Yan, Y. & Wang, C. Aβ42 is More Rigid than Aβ40 at the C Terminus: Implications for Aβ Aggregation and Toxicity. J Mol Biol. 2006;364(5):853–862.

29. Breydo, L. & Uversky, V.N. Structural, morphological, and functional diversity of amyloid oligomers. FEBS Lett. 2015;589(19): 2640–2648.

30. Dingemanse, J., Danhof, M., & Breimer, D.D. Pharmacokinetic-pharmacodynamic modeling of CNS drug effects: An overview. Pharmacol Ther. 1988;38(1):1–52.

31. Janelidze, S., *et al.* CSF Aβ42/Aβ40 and Aβ42/Aβ38 ratios: better diagnostic markers of Alzheimer disease. Ann Clin Transl Neurol. 2016;3(3):154–65.

32. Lomakin, a., Chung, D.S., Benedek, G.B., Kirschner, D.a., & Teplow, D.B. On the nucleation and growth of amyloid beta-protein fibrils: detection of nuclei and quantitation of rate constants.. Proc Natl Acad Sci U S A. 1996;93(3):1125–1129.

Chapter 6

Supplemental Material

Supplement to

Systems pharmacology analysis of the Aβ oligomer response following β-secretase inhibition: Evidence for second-order Aβ42 oligomerization

E.M.T. van Maanen, T.J. van Steeg, J. Kalinina, M.S. Michener, M.J. Savage, M.E. Kennedy, J.A. Stone, M. Danhof

SUPPLEMENTAL MATERIAL

Study differences

The response data of Aβ40, Aβ42, sAPPβ and sAPPα from the recent BACE1 inhibitor study[1] (hereinafter referred to as study 1) and the current BACE1 inhibitor study (hereinafter referred to as study 2) following a dose of 125 mg/kg MBi-5 is depicted in Supplemental Figure S6.1. A large between-study variability in the data was observed. This is also apparent from the plots of the ratios of Aβ42:Aβ40 (Supplemental Figure S6.2A), Aβ40:sAPPβ (Supplemental Figure S6.2B) and sAPPβ:sAPPα (Supplemental Figure S6.2C) in each study. There was no overlap in the rhesus monkey individuals included in studies 1 and 2.

References

1. van Maanen, E.M.T., *et al.* Systems Pharmacology Analysis of the Amyloid Cascade after β-Secretase Inhibition Enables the Identification of an Aβ42 Oligomer Pool. J Pharmacol Exp Ther. 2016;357(1):205–16.

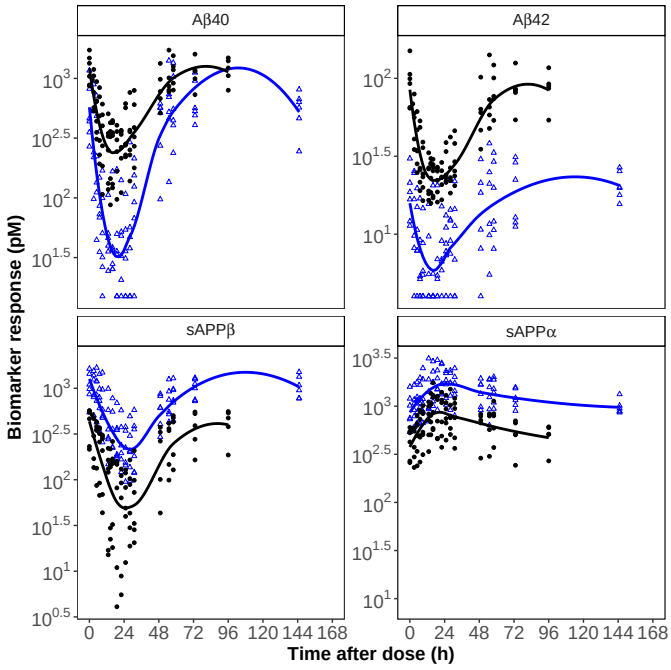

Figure S6.1: Study differences in absolute concentrations of biomarkers.
Study 1: blue line and symbols; Study2: black line and symbols; Lines are smoothers.

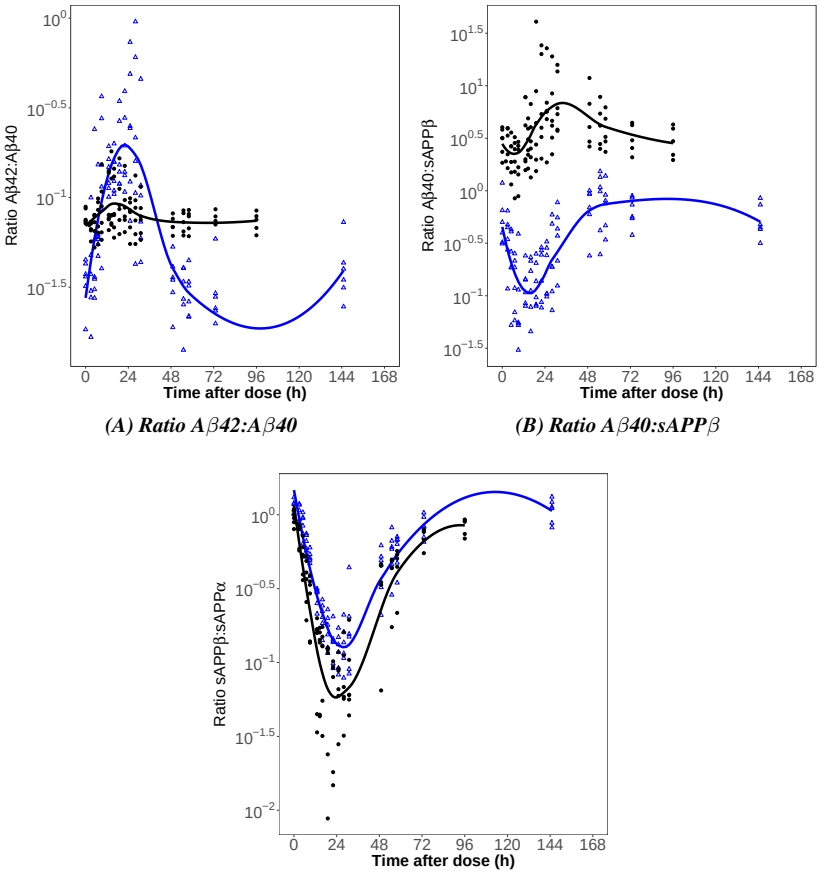

(A) Ratio Aβ42:Aβ40 ***(B) Ratio Aβ40:sAPPβ***

(C) Ratio sAPPβ:sAPPα

Figure S6.2: Study differences in ratios of biomarkers.
Study 1: blue line and symbols; Study2: black line and symbols; Lines are smoothers.